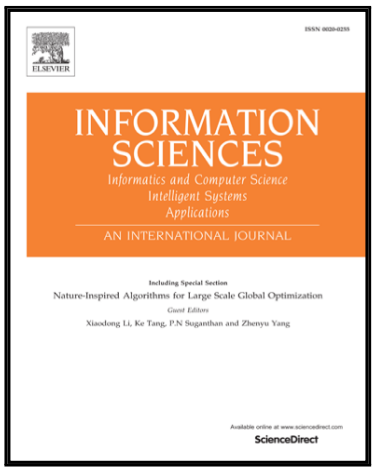

Local Gradient Patterns (LGP): An Effective Local-Statistical-Feature Extraction Scheme for No-Reference Image Quality Assessment

Wujie Zhou , Lu Yu , Weiwei Qiu , Yang Zhou , Mingwei Wu

PII: S0020-0255(17)30547-9
DOI: 10.1016/j.ins.2017.02.049
Reference: INS 12772

To appear in: *Information Sciences*

Received date: 25 March 2015
Revised date: 15 February 2017
Accepted date: 17 February 2017

Please cite this article as: Wujie Zhou , Lu Yu , Weiwei Qiu , Yang Zhou , Mingwei Wu , Local Gradient Patterns (LGP): An Effective Local-Statistical-Feature Extraction Scheme for No-Reference Image Quality Assessment, *Information Sciences* (2017), doi: 10.1016/j.ins.2017.02.049

Local Gradient Patterns (LGP): An Effective Local-Statistical-Feature Extraction Scheme for No-Reference Image Quality Assessment

Wujie Zhou[a,c*], Lu Yu[b], Weiwei Qiu[a], Yang Zhou[a], Mingwei Wu[a]

[a] *School of Information and Electronic Engineering, Zhejiang University of Science and Technology, Hangzhou 310023, China*

[b] *College of Information Science and Electronic Engineering, Zhejiang University, Hangzhou 310027, China*

[c] *School of Automation, Hangzhou Dianzi University, Hangzhou 310018, China*

ABSTRACT

Gradient features are known to be effective for full-reference (FR) image quality assessment (IQA). However, only a few metrics utilize gradient features for no-reference (NR) IQA. To investigate the potential benefits of gradient magnitude and phase for NR-IQA, we propose a novel and effective local-statistical-feature extraction metric, namely Local Gradient Patterns (LGP), for general-purpose NR-IQA. Using a Gaussian partial derivative filter, the image is first decomposed into two complementary components: gradient magnitude and phase. The local statistical features (e.g., the conditional probability distributions) are then extracted from the complementary components, using the derived local gradient magnitude and phase pattern operators. Finally, to facilitate NR-IQA, local statistical features that convey important structural information are mapped to the subjective mean opinion score of the image, using a support vector regression (SVR) procedure. We evaluated our proposed LGP metric using images from two publicly available test databases; the results confirm that the proposed LGP metric provides predictive performance that is superior to most state-of-the-art NR-IQA metrics and has an acceptable level of computational complexity.

Keywords: No-reference image quality assessment, local gradient patterns, gradient magnitude and phase, local statistical features, support vector regression.

1. Introduction

Image quality assessment (IQA), as one of the most common (yet very challenging) applications of image analysis and understanding, has drawn significant attention in many areas owing to its importance in various multimedia applications, including image acquisition, transmission, storage, compression, restoration, and enhancement [33]. Research on IQA can be broadly divided into subjective and objective methods. The former methods are based on subjective judgments by human viewers, and the latter methods drive an objective metric to quantify the perceived quality of a distorted image. Although subjective IQA provided by end users is the most accurate and straightforward method for quantifying perceived quality, it has a number of limitations: it is time- and labor-intensive, it is cumbersome, and it cannot be conducted in real time in automated systems [48, 37]. Hence, efforts to develop objective IQA metrics have been increasing annually. Objective IQA

*Corresponding author.

E-mail addresses: wujiezhou@163.com (W. Zhou)

Postal address: 310023

Tel.:+86-571-85070300.

can be further classified into full-reference (FR), reduced-reference (RR), and no-reference (NR), according to the accessibility of the pristine natural image [1]. Recently, FR-IQA has achieved satisfactorily effective levels of performance, as demonstrated by high correlations with human subjective perception. Structural similarity (SSIM) [29], multi-scale SSIM (MS-SSIM) [32], visual information fidelity (VIF) [24], feature similarity (FSIM) [44], matching pursuit-based FR-IQA [5], and gradient magnitude similarity deviation (GMSD) [36] are examples of successful and sophisticated FR-IQA metrics. However, the application scope of FR metrics is rather limited, because the original signal is unavailable in many scenarios. For these cases, it is important to devise NR-IQA metrics that can, in essence, emulate human subjective perception when quantifying a distorted image's perceived quality without having information describing the pristine natural image.

Existing mainstream NR-IQA can be divided into two main categories: distortion-specific NR-IQA and general-purpose NR-IQA [13, 12]. The former category can estimate the perceived quality of a distorted image only if its distortion types are known in advance; a considerable number of distortion-specific NR-IQA metrics, which each work well for one specific type of distortion, have been proposed [4, 7, 2, 40]. For example, in [4], Hassen *et al.* proposed a local phase coherence (LPC) -based metric that can measure perceived image blurriness/sharpness without analyzing the pristine natural image. In [7], Huang *et al.* proposed an NR noisy IQA metric based on estimated noise variance. Moreover, distortion-specific NR-IQA metrics have been developed specifically for JPEG compression distortion [2] and JPEG2000 compression distortion [40]. The obvious disadvantage of the above-mentioned NR-IQA metrics is that they are distortion specific, and hence application specific to some extent. Thus, it is beneficial to devise and refine general-purpose NR-IQA metrics that can quantify the perceived quality of a distorted image without advance knowledge of the distortion types.

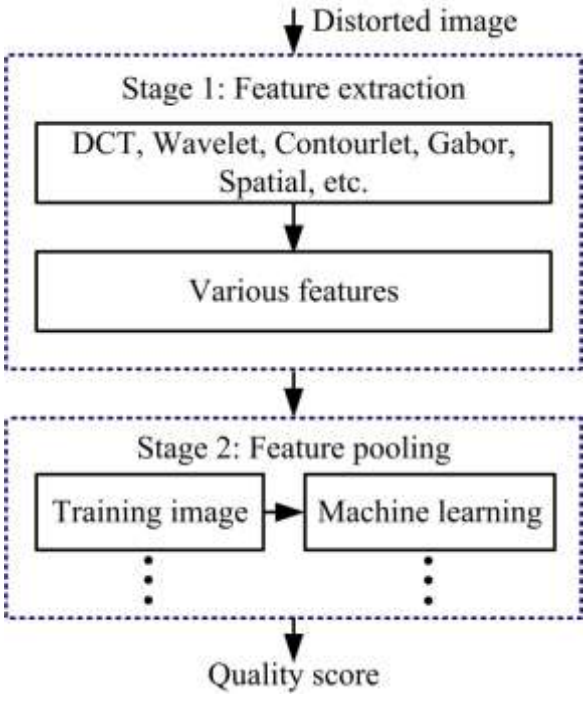

Fig. 1 Pipeline of the first type of general-purpose NR-IQA metrics

General-purpose NR-IQA metrics, which do not require knowledge of the distortion types, have recently emerged [13]. General-purpose NR-IQA metrics can be mainly classified into two types. Fig. 1 shows a pipeline of the first type of general-purpose NR-IQA metrics. The figure shows that this metric type has two main stages: feature extraction and feature pooling. The processes in the feature extraction stage are based on the following observations: first, when the image is properly normalized or transferred to some transform domain (e.g., DCT [22], wavelet [18, 19], Gabor [38], shearlet [10], spatial [15, 34, 41]), local descriptors can be modeled by some feature distributions. Second, the shapes of these distributions are very different for distorted and non-distorted (natural) images. In the feature pooling stage, different regression techniques such as support vector regression (SVR) [28], general regression neural networks (GRNN)[9], and multiple kernel learning (MKL) [6] can be applied to learn the mapping from feature distributions (extracted in the feature extraction stage), in order to assess the image's perceived quality. Therefore, different feature extraction and feature pooling schemes lead to different NR-IQA metrics. For example, Saad *et al*. derived the blind image integrity notator (BLIINDS2) [22], an NR-IQA metric that utilizes DCT statistics; in this metric, a Bayesian probabilistic inference model is utilized to quantify the image's perceived quality score. Moorthy *et al*. [18] trained a support vector machine (SVM) [28] to detect image distortion types, using statistical models of a steerable pyramid transform. They subsequently trained an SVR model [28] to quantify the perceived severity of each distortion type; this was referred to as the blind image quality index (BIQI). A similar two-step framework called distortion identification-based image verity and integrity evaluation (DIIVINE), which includes distortion classification and quality prediction, is employed in [19], where several natural scene statistics (NSS) features are also extracted in the wavelet domain. In [38], Ye *et al*. proposed CORNIA to extract features from a Gabor-filter-based visual codebook and introduced two different strategies for regression. In [9], Li *et al*. developed an NR-IQA metric based on several complementary and perceptually relevant image features that are fed to a general regression neural network (GRNN). The second general-purpose NR-IQA metric type operates without training with manually rated distorted images. For instance, in [16], Mittal *et al.* proposed the natural image quality evaluator (NIQE), which does not require training with subject-rated distorted images. In [35], Xue *et al.* proposed a quality-aware clustering (QAC) metric that learns a set of centroids that are used as a codebook to calculate the quality of the patches in each image. Zhang *et al*. [43] developed an opinion-unaware NR-IQA metric by integrating natural-image-feature statistics derived from multiple cues. Moreover, in applications such as real-time image quality prediction and monitoring, the complexity of implemented NR-IQA metrics becomes crucial. To proactively reduce complexity, Mittal *et al*. [15] proposed an NSS-based NR-IQA metric, the blind/NR image spatial quality evaluator (BRISQUE), which operates in the spatial domain; experimental results suggest that BRISQUE is an ideal candidate for real-time blind measurement of image quality. Most recently, local structure features, which are closely related to perceived image quality, have proved to be efficient tools for NR-IQA [34, 41]. For example, in [34], Xue *et al*. proposed a novel NR-IQA metric that utilizes the joint statistical features of gradient magnitude (GM) and Laplacian of Gaussian (LOG). In [41], Zhang *et al*. proposed a new local structure descriptor to form an NR-IQA metric by utilizing a LOG filter. The two NR-IQA metrics [34, 41] described above have very low time complexity and can serve as appropriate candidates for real-time blind measurements of image quality. However, only the magnitude of structural information was considered for feature extraction; thus, the features do not reflect true visual perception. In general, the success of NR metrics is based on the types of quality-aware features that are used to quantify quality.

Recently, image gradient features such as magnitude and phase have proved to be reasonably simple and useful tools for shaping FR-IQA metrics [36, 42]; they can effectively capture an image's local semantic structures, to which human subjective perception is highly sensitive. However, for NR-IQA, only a few NR approaches utilize the magnitude features [10, 34] or phase features [4, 6]; these are fed to a general regression model for quantifying the perceived quality of images, whereas the magnitude and phase, which play complementary roles in representing semantic structural information are considered less frequently or ignored. In other words, there is limited research on general-purpose NR-IQA based on magnitude and phase features, despite the long-held and widely recognized fact that magnitude and phase represent the appearance of an image [3]. In recent years, there have been many attempts to use local gradient magnitude patterns in computer vision [23]. Islam proposed a novel technique that uses local gradient magnitude patterns for facial expression recognition [23]. Most previous works have focused on applying local gradient magnitude patterns to the pattern recognition problem; in this study, they are applied to NR-IQA. In designing our proposed metric, we also consider the potential of local gradient phase patterns as a complementary and effective quality-aware source of structural information. Thus, our current work complements prior work by using the image gradient magnitude and phase together for NR-IQA, rather than using the gradient magnitude or phase separately.

Feature extraction and selection are crucial in NR-IQA metrics design. To the best of our knowledge, this work is the first NR-IQA study to use *gradient magnitude* and *phase*, which are simple yet effective local statistical features that can play important complementary roles in general-purpose NR-IQA. The first contribution of our work is the derivation of two novel and powerful local structure descriptors, referred to as local gradient patterns (LGP). The second contribution is the use of local statistical features (e.g., the conditional probability distributions); these are extracted from the complementary components *gradient magnitude* and *phase* and employed as quality-aware statistical features to form a novel NR-IQA metric. Combining these two contributions provides a particularly potent and simple general-purpose NR-IQA metric. Experimental results on two publicly available databases demonstrate that the proposed LGP metric provides results that are significantly more consistent with human subjective judgments than are state-of-the-art NR-IQA metrics and well-known FR-IQA metrics (e.g., SSIM and FSIM). Furthermore, the proposed LGP metric is conceptually very simple and has relatively low computational complexity.

The remainder of this work is organized as follows. Section 2 provides details of the proposed LGP metric, including the local-statistical-feature extraction scheme and feature pooling strategy. Experimental results are discussed and analyzed in Section 3. Lastly, Section 4 concludes this work.

2. LGP: A Novel NR-IQA Metric

As stated in the introduction, gradient features are basic and inherent properties of human visual perception that are commonly employed to characterize the various local semantic structures of an image. As we will see, they are also strong and active features for quantifying the perceived quality of images. Specifically, the first step in the proposed LGP metric is to apply the Gaussian partial derivative filter to the distorted image to obtain two complementary components: gradient magnitude and phase. Next, two types of local statistical features are extracted: one type from the local gradient magnitude patterns and one type from the local gradient phase patterns. Finally, by utilizing support vector regression (SVR), these local statistical features are employed as quality-aware features for quantifying the perceived quality of images. The following section describes the

procedures of the local-statistical-feature extraction scheme and feature pooling strategy.

2.1. Gradient Magnitude and Phase

Recently, from a computational point of view, an image gradient that contains important edge information describing structure and configuration has been employed for FR-IQA in various manners [44, 36]. The gradient is defined as the convolution of the image using linear operators; i.e.,

$$G_{d,\sigma}(z) = I(z) * h_d(x, y \mid \sigma),\ d \in \{x, y\} \tag{1}$$

where "*" is the linear convolution operator, $I(z)$ denotes the input image, z is the position of the input image $I(z)$, and h_d denotes the Gaussian partial derivative filter:

$$\begin{aligned} h_d(x, y \mid \sigma) &= \frac{\partial}{\partial d} g(x, y \mid \sigma) \\ &= -\frac{1}{2\pi\sigma^2} \frac{d}{\sigma^2} \exp\left(-\frac{x^2 + y^2}{2\sigma^2}\right) \end{aligned} \tag{2}$$

In (2), σ is the scale parameter ($\sigma \in \{\sigma_1, \sigma_2\}$), which can be utilized to obtain semantic structures from an image. Previous works [30] revealed that the diverse scale, magnitude, and phase sensitivities of the classical receptive fields (CRF) can be closely modeled by a Gaussian derivative function.

For each Gaussian partial derivative filter, at every image position z, the partial derivatives $G_{x,\sigma}(z)$ and $G_{y,\sigma}(z)$ along the x and y directions can be calculated. Based on these two partial derivatives, the magnitude and phase of $G_{d,\sigma}(z)$, denoted by $A_\sigma(z)$ and $\varphi_\sigma(z)$, are respectively given by

$$A_\sigma(z) = \sqrt{[G_{x,\sigma}(z)]^2 + [G_{y,\sigma}(z)]^2} \tag{3}$$

and

$$\varphi_\sigma(z) = \arctan(G_{x,\sigma}(z) / G_{y,\sigma}(z)) \tag{4}$$

2.2. Local Gradient Magnitude and Phase Patterns

From Marr's theory [14], local semantic structural information, which contains primitives in the primary visual cortex (area V1), is closely related to the perceived quality of images; further, local semantic structural modifications can generally reflect degradations in image quality. Recent studies proved that local structure descriptors (e.g., local binary patterns (LBPs) [20]) can efficiently and effectively represent the local semantic structural information of an image and can be considered as the binary approximation of the local semantic structural information primitives in the primary stage of vision [11, 39]. When image structure degradation or distortion occurs, local statistical distributions, which are a result of the inherent dependence between adjacent pixels, will be altered accordingly. In previous works [41, 46, 45], LBP-based statistics have been employed for IQA in various manners and proved to be quite useful. Based on the aforementioned points, we aim to fulfill NR-IQA tasks by using local statistical features generated from the gradient magnitude and phase with the derived local

gradient magnitude and phase pattern operators.

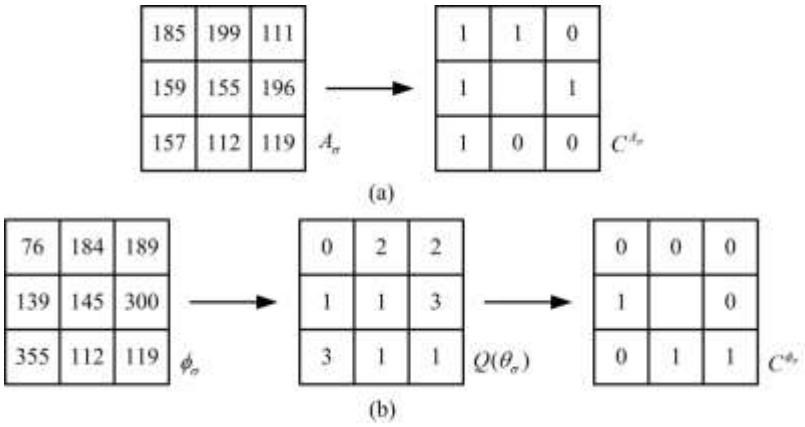

Fig.2 Binary quantification, (a) Binary quantification of gradient magnitude, (b) binary quantification of gradient phase.

Local binary structural patterns represented as “uniform” have been considered as the principal properties of local images [46, 45, 49]. A typical local rotation invariant “uniform” pattern coding usually includes the following three steps: binary quantification, binary sequence generation, and “uniform” pattern conversion. Among the procedures in local rotation invariant “uniform” pattern coding, the generation of binary sequences and the conversion of binary sequences to “uniform” patterns are common steps in most binary pattern coding schemes.

However, the first step of the local rotation invariant “uniform” pattern coding, i.e., binary quantification, usually relies on the characteristics of feature maps and should be devised based on the physical significance of the feature. According to the characteristics of local magnitude and phase, different binary quantification strategies are employed to generate the binary code [46, 45, 49].

1) Binary Quantification of Gradient Magnitude: Gradient magnitude is a measurement of local structural information and is closely related to the perceived quality of images. For example, high magnitude usually indicates high-energy local structural features (e.g., corners, edges, lines, and textures). When a perceptible image is distorted or damaged, the local structures will accordingly suffer degradation in gradient magnitude. Therefore, the local changes of magnitude, which reflect the variations in local quality degradation, can be quantified by comparing the magnitude value of a central location it shares with its neighbors, which is similar to an LBP [20]. For a local path (e.g., 3 × 3 neighborhood), let $A_\sigma(z_c)$ denote the magnitude value of the central pixel z_c, and let $A_\sigma(z_i)$ denote the magnitude value of the ith adjacent pixel z_i. Usually, we readjust the range of the magnitude to [0, 255]. Then, the magnitude binary quantification of the ith neighbor is defined as

$$C^{A_\sigma}(z_c - z_i) = \begin{cases} 1 & if\ A_\sigma(z_i) \geq A_\sigma(z_c) \\ 0 & else \end{cases} \tag{5}$$

The procedures to compute the binary quantification of the gradient magnitude are illustrated by an example in Fig. 2(a).

2) Binary Quantification of Gradient Phase: The gradient phase has been shown to be the primary contributor to the high-quality appearance of an image [46, 45, 49]. Phase changes generally lead to

significant perceived image distortion. In this paper, we first normalize the range of the gradient phases to [0, 360). It is more significant to compute the feature type than to directly compute the degree of the angle. Therefore, the binary quantification of the local gradient phase change should adopt a strategy different from that used for local gradient magnitude. Inspired by the LBP strategy, two cases should be considered when comparing the feature types: in the first case, the feature types are different; in the second, the feature types are similar to each other or the same. To improve the stability of binary quantification, the normalized ranges [0, 360) of phases are divided into *K* intervals (we set *K* = 4). The local feature types are considered to be similar when they belong to an identical interval; otherwise, they are considered to be different. For a local patch, let $\theta_\sigma(z_c)$ denote the local phase of the central pixel z_c, and let $\theta_\sigma(z_i)$ denote the phase of its *i*th neighbor. The gradient phase's binary quantification of the *i*th neighbor is defined as

$$C^{\phi_\sigma}(z_c - z_i) = \begin{cases} 1 & if\ Q(\theta_\sigma(z_c)) = Q(\theta_\sigma(z_i)) \\ 0 & else \end{cases}, \tag{6}$$

where $Q(\theta)$ is the phase quantification operator, defined as

$$Q(\theta) = q \quad if \quad \frac{360 \cdot (q-1)}{K} \le \theta < \frac{360 \cdot q}{K}. \tag{7}$$

The procedures for binary quantification of gradient phases are summarized in Fig. 2 (b).

Similar to the principle of the rotation invariant uniform LBP [20], the local rotation invariant patterns of the LGP can be written as

$$LGP_{\rho,R}^{\xi,riu2} = \begin{cases} \sum_{i=0}^{\rho-1} C^{\xi}(z_i - z_c) & if\ U(LGP_{\rho,R}^{\xi}) \le 2, \\ \rho + 1 & else \end{cases} \qquad \xi \in \{A_\sigma, \phi_\sigma\} \tag{8}$$

$$\begin{aligned} U(LGP_{\rho,R}^{\xi}) = & \left| C^{\xi}(z_{\rho-1} - z_c) - C^{\xi}(z_0 - z_c) \right| \\ & + \sum_{i=1}^{\rho-1} \left| C^{\xi}(z_i - z_c) - C^{\xi}(z_{i-1} - z_c) \right| \end{aligned}, \tag{9}$$

where ρ denotes the total number of involved neighbors, *R* denotes the radius of the neighborhood, and *U* denotes the frequency of 1-0 and 0-1 transitions in a circular representation of the LGP. There are $\rho + 2$ different bins of uniform LGPs to represent the structural distribution of the gradient features.

Then, the joint empirical probability function of $LGP_{\rho,R}^{A_\sigma,riu2}$ and $LGP_{\rho,R}^{\phi_\sigma,riu2}$ can be denoted by

$$
\begin{aligned}
T_{m,n}^{\sigma} &= P\left(LGP_{\rho,R}^{A_\sigma,riu2} = m, LGP_{\rho,R}^{\phi_\sigma,riu2} = n\right) \\
&= P\left(LGP_{\rho,R}^{A_\sigma,riu2} = m \mid LGP_{\rho,R}^{\phi_\sigma,riu2} = n\right) \cdot P\left(LGP_{\rho,R}^{\phi_\sigma,riu2} = n\right) \\
&= P\left(LGP_{\rho,R}^{\phi_\sigma,riu2} = n \mid LGP_{\rho,R}^{A_\sigma,riu2} = m\right) \cdot P\left(LGP_{\rho,R}^{A_\sigma,riu2} = m\right), m = 0,\cdots,\rho+1; n = 0,\cdots,\rho+1.
\end{aligned} \tag{10}
$$

Directly computing and using $T_{m,n}^{\sigma}$ to represent descriptive quality-aware features for NR-IQA is not an effective strategy because it has the same dimensions as the distorted image. In other words, although $T_{m,n}^{\sigma}$ contains a rich amount of statistical information regarding $LGP_{\rho,R}^{A_\sigma,riu2}$ and $LGP_{\rho,R}^{\phi_\sigma,riu2}$, it has high dimensionality. Instead, to capture the dependencies between gradient magnitude and phase, the conditional probability distributions, $P_C^{A_\sigma}$ and $P_C^{\phi_\sigma}$, which describe local image structures and the statistical interaction between $LGP_{\rho,R}^{A_\sigma,riu2}$ and $LGP_{\rho,R}^{\phi_\sigma,riu2}$, are written respectively as

$$
P_C^{A_\sigma}(LGP_{\rho,R}^{A_\sigma,riu2} = m) = \frac{\sum_{n=0}^{\rho+1} P(LGP_{\rho,R}^{A_\sigma,riu2} = m \mid LGP_{\rho,R}^{\phi_\sigma,riu2} = n)}{\rho+2} \tag{11}
$$

and

$$
P_C^{\phi_\sigma}(LGP_{\rho,R}^{\phi_\sigma,riu2} = n) = \frac{\sum_{m=0}^{\rho+1} P(LGP_{\rho,R}^{\phi_\sigma,riu2} = n \mid LGP_{\rho,R}^{A_\sigma,riu2} = m)}{\rho+2}. \tag{12}
$$

This allows us to eventually reduce multiple dimensions to one dimension. Finally, the conditional probability distributions are used as local statistical features, which can play a significant role in quantifying the perceived quality of images.

Fig. 3 Conditional probability distributions of natural images having different content. (a) Sailing; (b) Lighthouse; (c) Parrots; (d) Caps; (e) Monarch.

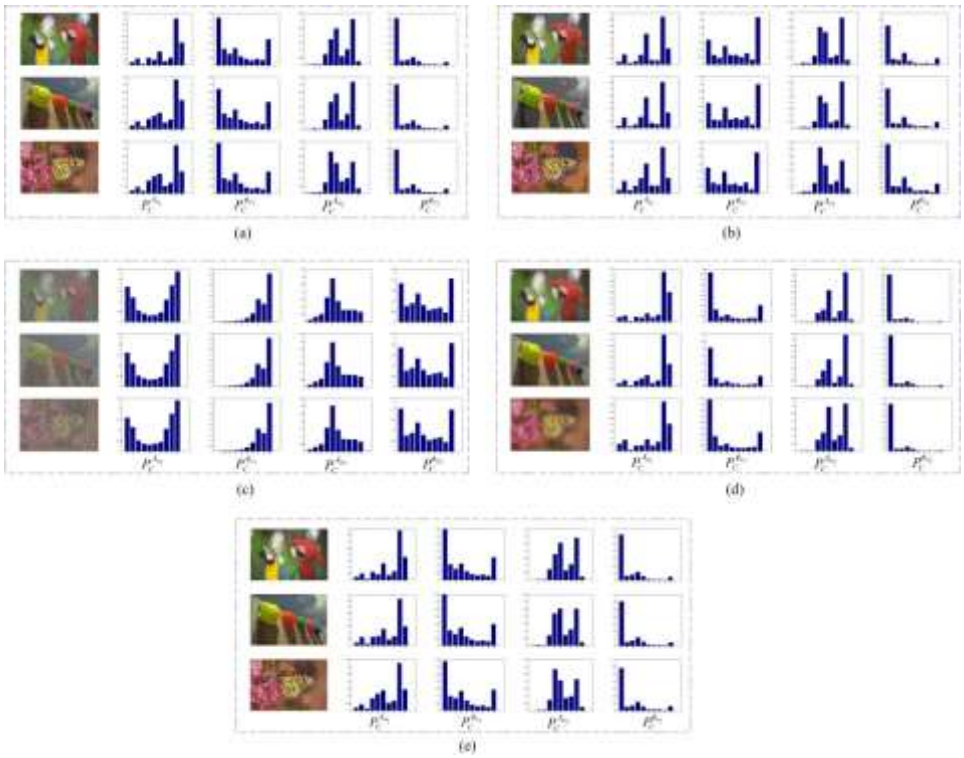

Fig. 4 Conditional probability distributions of distorted images for five distortion types with different image content. (a) JPEG2000 compression (JP2K); (b) JPEG compression (JPEG); (c) additive white noise (WN); (d) Gaussian blur (Gblur); (e) simulated fast fading Rayleigh channel (FF).

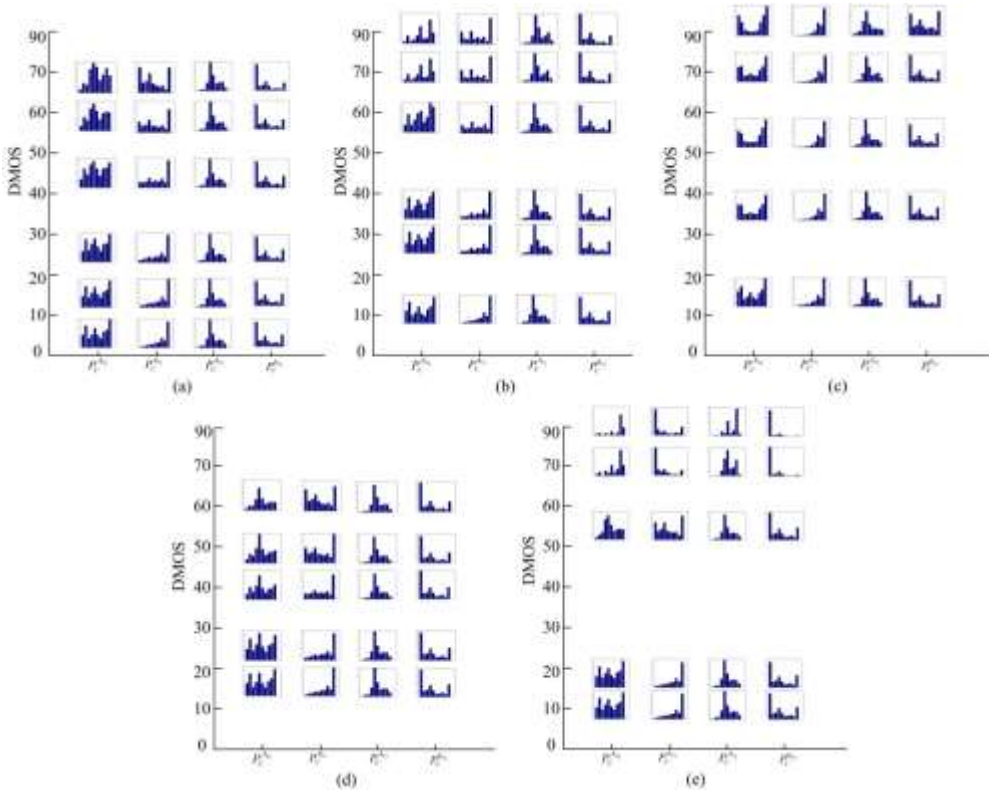

Fig. 5 Conditional probability distributions of distorted images at different distortion levels and showing their difference mean opinion scores (DMOSs). (a) JPEG2000 compression (JP2K), (b) JPEG compression (JPEG), (c) additive white noise (WN), (d) Gaussian blur (Gblur), (e) simulated fast fading Rayleigh channel (FF).

Fig. 3 shows the conditional probability distributions of natural images *Sailing, Lighthouse, Parrots, Caps,* and *Monarch*. It can be seen that the shapes of the conditional probability distributions are considerably consistent, despite their different natural image contents. In addition, Fig. 4 shows examples of conditional probability distributions of five distortion types with different image contents. As shown in Fig. 4, for images with varying image content but of the same distortion type, it is both very apparent and interesting that images with close difference mean opinion scores (DMOSs) share similar conditional probability distribution shapes. Therefore, we can conclude that content-independent conditional probability distributions are stable and feasible statistical quality-aware features for NR-IQA tasks. The above observations are the principal innovations and motivations of our proposed LGP metric.

To better illustrate how the types and levels of image distortions can affect the diverse conditional probability distributions of an image, we plot the conditional probability distributions across various DMOS values. Fig. 5 shows the conditional probability distributions of the natural image *Parrots* with different distortion types and levels. As shown in Fig. 5, when a natural image is distorted in an unnatural manner, some conditional probability distributions will deviate from those of a high-quality natural image. Further, one can see that the conditional probability distributions regularly change with increased levels of image distortion. In other words, the more serious the distortion is, the greater the alteration in the distribution plot. In addition, the alteration in the shapes of the conditional probability distributions caused by compression is very different from that caused by noise. Similar conclusions can be drawn for other distortion types. This shows that the shapes of the conditional probability distributions depend on the image distortion levels and on the perception of distortion. Thus, the conditional probability distributions can effectively capture the variations in local

structural information and can be appropriately applied for quantifying the perceived quality of images.

2.3. Quality Prediction

In order to map the features of an image to its DMOS, a statistical regression model is established in the quality prediction and feature pooling stage to learn a feature pooling strategy; this is accomplished using given feature vectors and training image DMOS values. Machine learning tools such as SVR [22, 18, 19, 38, 10, 15, 34, 41], GRNN [9], MKL [6], radial basis function neural networks (RBFNNs) [8,31], and random forest (RF) [27] can be used to learn the regression model. In this work, SVR with a radial basis function (RBF) kernel is adopted; this strategy employs the most widely used regression algorithm, and is highly effective for high-dimensional data pooling [22, 18, 19, 38, 10, 15, 34, 41]. With SVR, local statistical features are mapped to quality scores to train the quality prediction model, and the unknown f is constructed by linearly combining the results of a nonlinear transformation of the input samples.

$$f(\mathrm{x}) = \sum_{i=1}^{l} (\alpha_i - \alpha_i^*) \cdot k(\mathrm{x}_i, \mathrm{x}) + b \tag{13}$$

Here, α and α^* are the Lagrange multipliers, $k(\mathrm{x}_i, \mathrm{x}) = \exp(-\gamma(|\mathrm{x}_i - \mathrm{x}|)^2)$ is an RBF kernel, and γ is the precision parameter. More details regarding ε-SVR can be found in [28].

The prediction model learning process is illustrated by an example in Fig. 6. As shown in Fig. 6, the database is randomly split into two non-overlapping subsets: a training set and a test set.

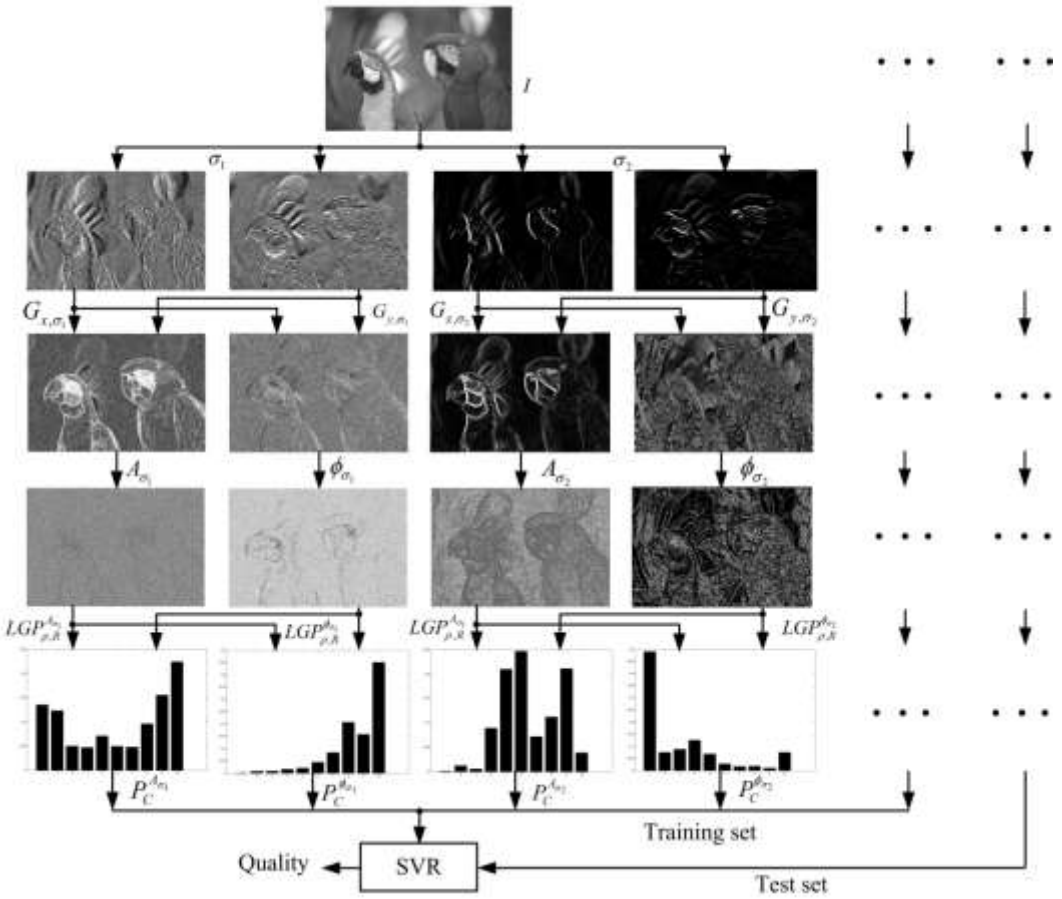

Fig. 6 Prediction model learning process.

3. Experiment Results and Discussion

3.1. Databases and Evaluation Indicator

In the experiments, two publicly available databases were utilized to verify the prediction performance of the proposed LGP metric. This section describes the test databases.

1) The LIVE database, created at the University of Texas [25], contains 799 distorted images and associated DMOS values generated from 29 pristine natural images distorted with five distortion types, at differing levels of distortion. The images in the LIVE database contain the following distortions: JPEG2000 compression (JP2K), JPEG compression (JPEG), additive white noise (WN), Gaussian blur (Gblur), and simulated fast fading Rayleigh channel (FF). These distortions reflect a broad range of image impairments, such as edge smoothing, additive random noise, block artifacts, and image-dependent distortions. A DMOS value, which represents a human perceptual judgment of the image, is provided for each distorted image.

2) The TID2008 database [21], from the Tampere University of Technology, is composed of 25 pristine natural images and their distorted counterparts with 17 categories of distortions; four different distortion levels are used. For the TID2008 database, we mainly considered the four categories of distortions in common with the LIVE database: JP2K, JPEG, WN, and Gblur. Moreover, the 25th pristine natural image (an artificial image) and related distorted images were not utilized, owing to their unnatural and synthesized texture.

Three commonly used performance indicators were employed to measure the prediction accuracy, prediction monotonicity, and prediction consistency of each IQA metric. The performance indicators were utilized in previous tests and recommended by the Video Quality Experts Group (VQEG). The computation of these indicators requires a regression procedure to reduce the non-linearity of predicted scores. Q_o, Q_p and Q_{DMOS} respectively denote the vectors of the original predicted scores before regression, the predicted scores after regression, and DMOS. The five-parameter logistic function that was used has the following form:

$$Q_p = a_1\left(\frac{1}{2} - \frac{1}{e^{a_2\times(Q_o - a_3)}}\right) + a_4 \times Q_o + a_5 , \tag{14}$$

where $\{a_1, a_2, a_3, a_4, a_5\}$ are model parameters obtained by utilizing a nonlinear logistic regression [26]. After the regression, three correspondence indicators can be computed for performance evaluation, as follows:

1) The first indicator is the Pearson linear correlation coefficient (PLCC) between Q_{DMOS} and Q_p. The PLCC value is defined as

$$PLCC = \frac{\sum (Q_p - \overline{Q_p})(Q_{DMOS} - \overline{Q_{DMOS}})}{\sqrt{\sum (Q_p - \overline{Q_p})^2 \sum (Q_{DMOS} - \overline{Q_{DMOS}})^2}} , \tag{15}$$

where $\overline{Q_p}$ and $\overline{Q_{DMOS}}$ are the mean-removed vectors of Q_p and Q_{DMOS}, respectively. PLCC is calculated to evaluate the prediction accuracy of IQA metrics.

2) The second indicator is the Spearman's rank order correlation coefficient (SROCC) between Q_o and $\overline{Q_{DMOS}}$, and computed by

$$SROCC = 1 - \frac{6 \times \sum_{i=1}^{N} d_i^2}{N(N-1)}, \tag{16}$$

where d_i is the difference between the *i*-th image's ranks in Q_{DMOS} and Q_o, and *N* is the total number of samples. Note that the logistic regression affects the SROCC indicator. SROCC can reflect the monotonic prediction of IQA metrics.

3) The last indicator is the root-mean-squared error (RMSE) between Q_p and Q_{DMOS}. This indicator is designed to evaluate the prediction consistency:

$$RMSE = \sqrt{\frac{1}{N}\sum (Q_p - Q_{DMOS})^2}. \tag{17}$$

Note that higher PLCC and SROCC values with lower RMSEs denote better correlation with human perception. A well-defined metric will generate a value close to 0 for RMSE and values close to 1 for PLCC and SROCC. More details (e.g., definition and explanation) regarding the three performance indicators can be found in [17] and [47].

3.2. Implementation of the Proposed LGP Metric

Various parameters must be determined for the proposed LGP metric. When computing the gradient features, the scales $\sigma \in \{\sigma_1, \sigma_2\}$ of the Gaussian partial derivative filter are selected as $\{\sigma_1 = 0.5, \sigma_2 = 2.5\}$. This allows fine image details to be captured in gradient magnitude and phase maps. In addition, when coding the binary quantifications of gradient magnitude and phase, computational efficiency must be considered; the objective is to obtain the highest possible prediction performance using as few features as possible. To meet this objective, in our experiments *ρ* and *R* were set to 8 and 1, respectively.

Table 1 Cross-validation experiment results

Parameter	LIVE	TID2008
C	8192	128
γ	2	4

Table 2 Comparison of performance of 10 IQA metrics on two benchmark databases

Dataset Indicator	FR	NR

		PSNR	SSIM	FSIM	BIQI	DIIVINE	BLIINDS2	CORNIA	BRISQUE	GM-LOG	LGP
LIVE	PLCC	0.8821	0.9464	0.9612	0.8250	0.8916	0.9366	0.9487	0.9468	0.9551	**0.9572**
(779	SROCC	0.8829	0.9486	0.9639	0.8084	0.8816	0.9302	0.9466	0.9430	0.9511	**0.9537**
images)	RMSE	12.8983	8.8035	7.5461	15.3883	12.3294	9.5185	8.6969	8.7214	8.0444	**7.9011**
TID2008	PLCC	0.8611	0.9087	0.9539	0.8704	0.9038	0.9219	0.9347	0.9391	0.9406	**0.9426**
(384	SROCC	0.8789	0.9032	0.9555	0.8438	0.8930	0.8982	0.8990	0.9357	**0.9369**	0.9258
images)	RMSE	0.8073	0.6620	0.4707	0.7872	0.6714	0.6117	0.5669	0.5442	0.5377	**0.5278**
Weight	PLCC	0.8752	0.9340	0.9588	0.8340	0.8956	0.9317	0.9441	0.9443	0.9503	**0.9524**
average	SROCC	0.8816	0.9336	0.9611	0.8201	0.8854	0.9196	0.9309	0.9406	**0.9464**	0.9445

Because the proposed metric employs the ε-SVR technique for NR-IQA, we iteratively divided each database into a test set (20%) and a training set (80%), with no content overlap between the sets. The LIBSVM package was utilized to execute the ε-SVR [28]. The train–test procedure was executed 1000 times, and the median results among those 1000 trials were chosen for the final evaluation results. When utilizing the ε-SVR to learn the regression models, the ε-SVR parameters (C, γ) must be set. To select the values of (C, γ), we used a grid search engine to conduct a cross-validation experiment. The (C, γ) parameters that delivered the best performance are summarized in Table 1.

3.3. Overall Performance Comparison

To more comprehensively validate the statistical performance of the proposed LGP metric, we compared it with other state-of-the-art and well-known objective metrics, including three FR-IQA metrics (PSNR, SSIM [29], and FSIM [44]) and six holistic NR-IQA metrics (BLIINDS2 [22], BIQI [18], DIIVINE [19], CORNIA [38], BRISQUE [15], and GM-LOG [34]) in terms of PLCC, SROCC, and RMSE. To conduct a fair comparison, we also optimized the SVR parameters for these NR metrics using a grid search. The 80% training–20% test procedure was also repeated 1000 times; the median results were then reported for performance evaluation. All IQA metrics were operated within the luminance component (the gray-scale version) of RGB color distorted images.

The PLCC, SROCC, and RMSE values generated by the proposed metric are listed in Table 2, for all distortion types in the LIVE database and TID2008 database. At the bottom of Table 2, we show the weighted-average PLCC and SROCC values generated by the competing IQA metrics, using the two databases. In each case, the results of the best-performing NR-IQA metric are marked in bold. The experimental results show that the proposed LGP metric provides relatively accurate image quality predictions, compared with other FR- and NR-IQA metrics. It delivers performance that is statistically superior to the most popular NR metrics, including DIIVINE, BLIINDS2, CORNIA, and BRISQUE. Its performance is slightly worse than FSIM; however, FSIM is a top-performing FR method, whereas our proposed metric is an NR method. Specifically, in terms of prediction accuracy (PLCC and RMSE), the proposed LGP metric consistently provides high performance in tests on the two databases; in terms of prediction monotonicity (SROCC), the proposed LGP metric is statistically close to the top-performing NR-IQA metric (GM-LOG). In summary, the proposed LGP metric is an accurate, robust, and consistently objective NR-IQA metric for predicting the perceived quality of a distorted image.

Table 3 Performance comparison of 10 IQA metrics for each individual distortion type

Distortion	FR			NR						
	PSNR	SSIM	FSIM	BIQI	DIIVINE	BLIINDS2	CORNIA	BRISQUE	GM-LOG	LGP

LIVE	JP2K	0.8954	0.9614	0.9717	0.7849	0.8418	0.9258	**0.9271**	0.9175	**0.9283**	**0.9509**
	JPEG	0.8809	0.9764	0.9834	0.8801	0.8926	0.9500	0.9437	**0.9655**	**0.9659**	**0.9652**
	WN	0.9854	0.9694	0.9652	0.9157	0.9617	0.9477	0.9608	**0.9789**	**0.9853**	**0.9782**
	Gblur	0.7823	0.9517	0.9708	0.8367	0.8792	0.9132	**0.9553**	**0.9479**	0.9395	**0.9430**
	FF	0.8907	0.9556	0.9499	0.7023	0.8202	0.8736	**0.9103**	0.8854	**0.9008**	**0.9119**
TID2008	WN	0.9114	0.8107	0.8566	0.5368	0.7130	0.7314	0.5941	**0.8603**	**0.9068**	**0.8211**
	GB	0.8682	0.9544	0.9472	0.8878	0.8824	**0.9176**	0.8941	**0.9059**	0.8812	**0.9143**
	JPEG	0.9011	0.9252	0.979	0.8996	0.9033	0.8853	0.9099	**0.9103**	**0.9338**	**0.9203**
	JP2K	0.8300	0.9625	0.9773	0.8147	0.9103	0.9188	**0.9290**	0.9044	**0.9263**	**0.9414**

3.4. Performance on Individual Distortion Types

To more comprehensively measure the generalization ability of IQA metrics and to predict the perceived quality of a distorted image degraded by some specific types of distortion, in this experiment we report the performance of the representative and prominent metrics for different individual distortion types. To conserve space, only the results for SROCC (the evaluation indicator) are shown in Table 3. By utilizing the other indicators, such as PLCC and RMSE, similar conclusions can be drawn. For each database and each type of distortion, the three NR-IQA metrics producing the highest performance (SROCC) are shown in bold font. As shown in Table 3, the proposed LGP metric ranks among the top three metrics nine times, followed by GM-LOG (seven times) and BRISQUE (six times). Although certain NR-IQA metrics may be more effective for some special types of distortion, the proposed LGP metric is quite competitive with the best metric for each distortion type.

3.5 Statistical Significance Testing

To evaluate the proposed LGP metric's statistically significant advantages over other competing NR-IQA metrics, a one-sided *t*-test was conducted at the 5% significance level, using the SROCC values obtained from the 1000 train–test trials. The null hypothesis is that the SROCC values for two metrics are taken from equal-mean populations, whereas the alternative hypothesis is that the mean of one metric is greater than that of the other metric. To guarantee the independency assumption of the *t*-test, the database was randomly split into training and test sets.

The results of the one-sided *t*-test (with a confidence of 95%) are tabulated in Table 4 and Table 5. A score of “1” in the tables indicates that the row metric is statistically better than the column metric, a score of “-1” indicates that the column metric is statistically better, and a score of “0” indicates that the two metrics are statistically indistinguishable. It is clear that the best performance was achieved by our proposed LGP metric, whose results are “1” in most cases. Specifically, the experimental results show that the proposed LGP metric is statistically superior to the competing NR-IQA metrics in tests on the LIVE database and is statistically similar to the NR approach GM-LOG in tests on the TID2008 database. In general, the proposed LGP metric achieves statistically better performance than other NR-IQA metrics.

Table 4 Results of one-sided *t*-test comparing SROCC values of various metrics (LIVE)

	BIQI	DIIVINE	BLIINDS2	CORNIA	BRISQUE	GM-LOG	LGP

BIQI	0	-1	-1	-1	-1	-1	-1
DIIVINE	1	0	-1	-1	-1	-1	-1
BLIINDS2	1	1	0	-1	-1	-1	-1
CORNIA	1	1	1	0	0	-1	-1
BRISQUE	1	1	1	0	0	-1	-1
GM-LOG	1	1	1	1	1	0	-1
LGP	1	1	1	1	1	1	0

Table 5 Results of one-sided *t*-test comparing SROCC values of various metrics (TID2008)

	BIQI	DIIVINE	BLIINDS2	CORNIA	BRISQUE	GM-LOG	LGP
BIQI	0	-1	-1	-1	-1	-1	-1
DIIVINE	1	0	-1	-1	-1	-1	-1
BLIINDS2	1	1	0	1	-1	-1	-1
CORNIA	1	1	-1	0	-1	-1	-1
BRISQUE	1	1	1	1	0	-1	0
GM-LOG	1	1	1	1	1	0	0
LGP	1	1	1	1	0	0	0

3.6. Database Dependency

In the experiments described in subsections 3.3 and 3.4, the training set and test set for each experiment were selected from the same database (i.e., the proposed LGP metric was evaluated on either the LIVE database or a selected portion of the TID2008 database). To ascertain whether the metric is database dependent (the training process is universal), the statistical regression model learned from one database should be tested on the other database. Therefore, to certify the generality and robustness of an NR-IQA metric, the statistical regression model learned from one database should be applied to another database to determine if satisfactory results can still be obtained. To test this, we conducted the following experiments. First, a statistical regression model was trained on the LIVE database; the learned model was then tested on the TID2008 database. Next, the statistical regression model was trained on the TID2008 database, and tested on the LIVE database. The SROCC indicator was utilized for evaluation and the cross-validation results are reported in Table 6. Again, the proposed LGP metric provided consistently high competitive performance. It achieved superior SROCC values, and its results are very close to the optimal results in all tests.

Table 6 Performance of NR-IQA metrics across the two databases

Database for training	Database for testing	BIQI	DIIVINE	BLIINDS2	CORNIA	BRISQUE	GM-LOG	LGP
LIVE	TID2008	0.8914	0.8599	0.9056	0.8932	0.9050	**0.9204**	**0.9082**
TID2008	LIVE	0.7631	0.8658	**0.9389**	0.9091	0.9288	**0.9336**	0.9195

Table 7 Execution times of the competing NR-IQA metrics

Metric	Feature domain	Feature length	Running times (s)
DIIVINE	Wavelet	88	94.92
BLIINDS2	DCT	24	417.1

CORNIA	Gabor	20000	10.93
BRISQUE	Spatial	36	0.59
GM-LOG	Gradient and LOG	40	0.34
LGP	Gradient	40	1.45

3.7. Complexity Analysis

The NR-IQA metrics' execution time is an important factor in evaluating the practicability of the proposed LGP metric, to facilitate its use in *real-time applications* such as image quality prediction, adjustment, and monitoring. The time complexity of general-purpose NR-IQA includes time consumed by feature extraction and feature pooling. The latter relies on the feature length, because the time complexity of SVR is based on the quadratic of the training set (this is why we do not directly use $T_{m,n}^{\sigma}$, which has the same dimensions as the distorted image). As shown in Table 7, the proposed LGP metric uses only 40 features. In this experiment, we mainly consider the time consumed by the extraction of local statistical features. We compared the efficiency (i.e., computational complexity) of the proposed LGP metric with other NR-IQA metrics (executing as unoptimized MATLAB code in order to ensure a fair comparison) using a Windows 7 PC with a 2.70 GHz Intel Core i5 processor and 8 GB RAM. The software platform was MATLAB version R2008a. The results are also listed in Table 7, in which we present the average time (in seconds) taken per image, over all the images from the LIVE database. These measurements provide a rough estimate of the relative computational complexity between different NR-IQA metrics. As Table 7 clearly shows, the proposed LGP metric executes more slowly than GM-LOG and BRISQUE. This is mainly because of a relatively time-consuming process required for capturing the local statistical features. However, the proposed LGP metric requires only 1.45 seconds to process an image, which is 9.48 times faster than CORNIA; at this speed, the proposed metric can generally meet the demands of real-time applications. In comparison, DIIVINE and BLIINDS2 require significantly more processing time than the proposed LGP metric.

4. Conclusion and Future Work

To facilitate the use of no-reference (NR) image quality assessment (IQA) methods, this study analyzed the usefulness and effectiveness of two complementary image components: gradient magnitude and phase. To the best of our knowledge, no previous studies have analyzed these components for use with NR-IQA. The novelty of this work is represented by an innovative local-statistical-feature extraction scheme called Local Gradient Patterns (LGP). This scheme facilitates NR-IQA by mapping local statistical features to the subjective mean opinion score of images. Experimental results obtained from tests on two publicly available databases demonstrate that, compared with competing metrics, the proposed LGP metric delivers much higher consistency in terms of alignment with human subjective judgments. It is competitive with the top-performing NR-IQA metric and outperforms other popular FR-IQA metrics, including PSNR and SSIM.

In the future, there are many important issues that deserve further exploration and investigation; these include 1) further research on gradient feature applications, 2) extraction of local statistical features from other magnitudes and phases for NR-IQA, 3) extension of the proposed LGP metric to facilitate video quality assessments and stereoscopic IQA, and 4) designing of more effective and efficient regression models for NR-IQA.

Acknowledgements

This research is supported by the National Natural Science Foundation of China (Grant Nos. 61502429, 61505176, 61431015, 61371162, 61302112), the Zhejiang Open Foundation of the Most Important Subjects, and the China Postdoctoral Science Foundation (Grant No. 2015M581932).

References

[1] A. Celotto, V. Loia, S. Senatore, Fuzzy linguistic approach to quality assessment model for electricity network infrastructure, Information Sciences, 304 (2015) pp. 1–15.

[2] S. Corchs, F. Gasparini, and R. Schettini, No reference image quality classification for JPEG-distorted images, Digital Signal Processing, 30 (2014) pp. 86–100.

D. J. Field and D. M. Chandler. Method for estimating the relative contribution of phase and power spectra to the total information in natural-scene patches, J. Opt. Soc. Am. A, 29 (2012) pp.55–67.

[3] R. Hassen, Z. Wang, and M. M. A. Salama. Image sharpness assessment based on local phase coherence. IEEE Transactions on Image Processing, 22 (2013) pp.2798–2810.

[4] R. C. Hong, J. X. Pan, S. J. Hao, M. Wang, F. Xue, X. D. Wu, Image quality assessment based on matching pursuit, Information Sciences, 273 (2014) pp. 196–211.

[5] W. L. Hou, X. B. Gao, D. C. Tao, and X. L. Li. Universal blind image quality assessment metrics via natural scene statistics and multiple kernel learning, IEEE Trans. on neural networks and learning systems, 24 (2013) pp. 2013–2026.

[6] X. T. Huang, L. Chen, J. Tian, X. L. Zhang, and X. W. Fu. Blind noisy image quality assessment using block homogeneity, Computers and Electrical Engineering, 40 (2014) pp. 796–807.

Y. Kokkinos and K. G. Margaritis, Topology and simulations of a hierarchical markovian radial basis function neural network classifier, Information Sciences, 294 (2015) pp. 612–627.

[7] C. Li, A. C. Bovik, and X. Wu, Blind image quality assessment using a general regression neural network, IEEE Trans. Neural Netw., 22 (2011) pp. 793–799.

[8] Y. Li, L. Po, X. Xu, and L. Feng, No-reference image quality assessment using statistical characteriaztion in the shearlet domain, Signal Processing: Image Communication, 29 (2014) pp. 748–759.

P. Liu, J. M. Guo, K. Chamnongthai, and H. Prasetyo, Fusion of color histogram and LBP-based features for texture image retrieval and classification, Information Sciences, (2017) http://dx.doi.org/10.1016/j.ins.2017.01.025

[9] Q. Lu, W. Zhou, H. Li, A no-reference image sharpness metric based on structural information using sparse representation, Information Sciences, 369 (2016) pp. 334-346.

[10] R. A. Manap, and L. Shao, Non-distortion-specific no-reference image quality assessment: A survey, Information Sciences, 301 (2015) pp. 141–160.

D. Marr,Vision.SanFrancisco, CA, USA: W.H. Freeman, 1980.

[11] A. Mittal, A. K. Moorthy, A. C. Bovik, No-Reference image quality assessment in the spatial domain, IEEE Trans. Image Process., 21 (2012) pp.4695–4708.

[12] A. Mittal, R. Soundararjan, A. C. Bovik, Making a 'completely blind' image quality analyzer, IEEE Signal Process. Lett., 20 (2013) pp.209–201.

A. K. Moorthy and A. C. Bovik, Visual importance pooling for image quality assessment, IEEE J. Sel. Topics Signal Process., 3 (2009) pp. 193–201.

[13] A. K. Moorthy and A. C. Bovik. A two-step framework for constructing blind image quality indices, IEEE Signal Process. Lett., 17 (2010) pp. 51–516.

[14] A. K. Moorthy and A. C. Bovik, Blind image quality assessment: From natural scene statistics to perceptual quality, IEEE Trans. on Image Process., 20 (2011) pp. 3350–3364.

T. Ojala, M. Pietikinen, and T. Menp, Multiresolution gray-scale and rotation invariant texture classification with local binary patterns, IEEE Trans. on Pattern Analysis and Machine Intelli., 24 (2002) pp. 971–987.

N. Ponomarenko, V. Lukin, A. Zelensky, K. Egiazarian, M. Carli, F. Battisti, TID2008 - A Database for Evaluation of Full-Reference Visual Quality Assessment Metrics, Advances of Modern Radio Electronics, 10 (2009) pp.30–45.

[15] M. A. Saad, A. C. Bovik, and C. Charrier, Blind image quality assessment: A natural scene statistics approach in the DCT domin, IEEE Trans. on Image Process., 21 (2012) pp. 3339–3352.

M. Shahidol Islam. Local gradient pattern-A novel feature representation for facial expression recognition, Journal of AI and Data Mining, 2 (2014) pp.33–38.

[16] H. Sheikh and A. Bovik, Image information and visual quality, IEEE Trans. Image Process., 15 (2006) pp. 430–444.

H. R. Sheikh, Z. Wang, L. Cormack, and A. C. Bovik, Live Image Quality Assessment Database Release 2, [Online]. http://live.ece.utexas.edu/research/quality.

H. R. Sheikh, M. F. Sabir, and A.C. Bovik, A statistical evaluation of recent full reference image quality assessment algorithms, IEEE Trans. Image Process., 15 (2006) pp. 3440–3451.

K. Singh, S. C. Guntuku, A. Thakur, and C. Hota, Big data analytics framework for peer-to-peer botnet detection using random forests, Information Sciences, 278 (2014) pp. 488–497.

A. J. Smola and B. Schölkopf, A tutorial on support vector regression, Statist. Comput., 14 (2004) pp. 199–222.

[17] Z. Wang, A. C. Bovik, H. R. Sheikh, and E. P. Simoncelli, Image quality assessment: From error visibility to structural similarity, IEEE Trans. Image Process., 13 (2004) pp. 600–612.

H. Wang, T. Z. Huang, Z. Xu, Y. Wang, An active contour model and its algorithms with local and global Gaussian distribution fitting energies, Information Sciences, 263 (2014) pp. 43–59.

Z. Wang, M. Li, and J. Li, A multi-objective evolutionary algorithm for feature selection based on mutual information with a new redundancy measure, Information Sciences, 307 (2015) pp. 73–88.

[18] Z. Wang, E. Simoncelli, and A. Bovik, “Multiscale structural similarity for image quality assessment,” in Proc. 37th Asilomar Conf. Signals, Syst. Comput. Conf. Rec., 2 (2003) pp. 1398–1402.

[19] J. Wu, W. Lin, G. Shi, L. Li, Y. Fang, Orientation selectivity based visual pattern for reduced-reference image quality assessment, Information Sciences, 351 (2016) pp. 18–29.

[20] W. F Xue, X. Q. Mou, L. Zhang, A. C. Bovik, and X. C. Chu. Blind image quality assessment using joint statistics of gradient magnitude and laplacian features, IEEE Trans. Image Process., 23 (2014) pp.4850–4862.

[21] W. Xue, L. Zhang, and X. Mou, Learning without human scores for blind image quality assessment, in Proc. IEEE Conf. Comp. Vis. Pattern Recog., (2013) pp.995–1002.

[22] W. F. Xue, L. Zhang, X. Q. Mou, and A. C. Bovik, Gradient magnitude similarity deviation: A highly efficient perceptual image quality index, IEEE Trans. Image Process., 23 (2014) pp. 684–695.

[23] J. Yang, Y. Wang, B. Li, W. Lu, Q. Meng, Z. Lv, Z. Gao, Quality assessment metric of stereo images considering cyclopean integration and visual saliency, Information Sciences, 373 (2016) pp. 251–268.

[24] P. Ye, J. Kumar, L. Kang, D. Doermann, Unsupervised feature learning framework for no-reference image quality assessment, in IEEE Conference on Computer Vision and Pattern Recognition, (2012) pp. 1098–1105.

F. Yuan, J. Shi, X. Xia, Y. Fang, Z. Fang, T. Mei, High-order local ternary patterns with locality preserving projection for smoke detection and image classification, Information Sciences, 372 (2016) pp. 225–240.

[25] J. Zhang, and T. M. Le, A new no-reference quality metric for JPEG2000 images, IEEE Trans. Consum. Electron., 56 (2010) pp. 743–750.

[26] M. Zhang, C. Muramatsu, X. R. Zhou, T. Hara, and H. Fujita. Blind image quality assessment using the joint statistics of generalized local binary pattern, IEEE Signal Process. Lett., 22 (2015) pp. 207–210.

L. Zhang, Y. Shen, H. Y. Li, VSI: A visual saliency induced index for perceptual image quality assessment, IEEE Trans. Image Process., 23 (2014) pp. 4270–4281.

[27] L. Zhang, L. Zhang, and A. C. Bovik, A feature-enriched completely blind image quality evaluator, IEEE Trans. on Image Processing, 24 (2015) pp.2579–2591.

[28] L. Zhang, D. Zhang, and X. Q. Mou, FSIM: a feature similarity index for image quality assessment, IEEE Trans. Image Process., 20 (2011) pp. 2378–2386.

W. Zhou, W. Qiu, M. W. Wu, Utilizing dictionary learning and machine learning for blind quality assessment of 3-D images, IEEE Transactions on Broadcasting, 63 (2017) https://doi.org/10.1109/TBC.2016.2638620

W. Zhou, L. Yu, Binocular responses for no-reference 3D image quality assessment, IEEE Transactions on Multimedia, 18 (2016) pp. 1007–1014.

W. Zhou, L. Yu, W. Qiu, T. Luo, Z. Wang, M. W. Wu, Utilizing binocular vision to facilitate completely blind 3D image quality measurement, Signal Processing, 129 (2016) pp. 130–136.

[29] W. Zhou, S. Zhang, T. Pan, L. Yu, W. Qiu, Y. Zhou, and T. Luo, Blind 3D image quality assessment based on self-similarity of binocular features, Neurocomputing, 224 (2017) pp.128–134.

J. Zou, W. Li, C. Chen, Q. Du, Q. Scene classification using local and global features with collaborative representation fusion, Information Sciences, 348 (2016) pp.209–226.